Fast Harmonic Balance of SIS Mixers with Multiple Junctions and Superconducting Circuits

Frank Rice, John Ward, Jonas Zmuidzinas, and Goutam Chattopadhyay

California Institute of Technology, 320-47, Pasadena, CA 91125, USA.

Abstract

We have extended the spectral domain harmonic balance method of Withington and Kollberg [1] to handle quasiparticle mixer circuits of arbitrary complexity containing any number of superconducting tunnel junctions. Our algorithm uses a multidimensional Newton-Raphson technique to achieve rapid convergence, even when many harmonics are included in the analysis. Another improvement is to perform all linear circuit calculations using the scattering matrix representation typical of modern circuit modeling techniques. This algorithm has been implemented as part of an extensive C++ class library for modeling the signal and noise performance of superconducting heterodyne receivers (SuperMix). Using the common, free C++ compiler "g++" (Free Software Foundation), impressive results can be achieved on modern workstations of moderate capability. Such speeds will make complex nonlinear optimization calculations a routine part of SIS receiver design.

I. Introduction

As the state of the art in submillimeter wave heterodyne mixers utilizing superconductor-insulator-superconductor (SIS) devices has progressed, SIS mixers are rapidly evolving to ever more complex and wide bandwidth designs. Examples include a sideband separating mixer [2], distributed junction arrays [3], and a dual-polarization receiver [4]. Additionally, the quest for wide IF bandwidth is spurring several investigations regarding the design of integrated SIS/HEMT receiver systems. To successfully optimize the performance of such sophisticated designs, accurate and efficient software modeling is required. Correctly calculating the complex interactions of the nonlinear responses of multiple SIS junctions will be vital to the success of such modeling. Consequently such software must include a fast and accurate harmonic balance method.

The small signal response of an electronic circuit containing nonlinear elements, such as a mixer, obtains from a perturbation analysis of the operating state. The operating state is determined by the large signal voltage and current waveforms across the nonlinear elements. Clearly it is essential to accurately determine these waveforms in order to proceed with the small signal analysis. The harmonic balance technique is a well established method for determining these large-signal waveforms.

For the purposes of harmonic balance, a network involving two-terminal nonlinear devices is normally modeled as in figure 1. Each nonlinear device is connected to its own port in the linear embedding network; the network includes dc and ac sources. The goal of harmonic balance is to determine the voltage and current waveforms $v(t)$ and $i(t)$ at each nonlinear device, thereby fixing its operating state and resultant small signal behavior. Traditionally harmonic balance proceeds by analyzing the linear

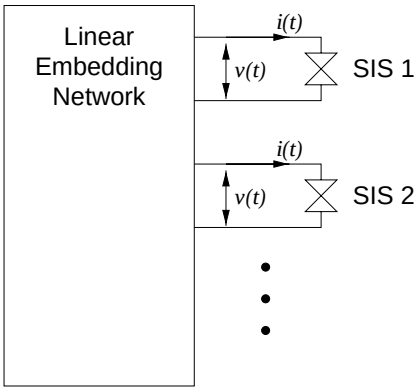

Fig. 1. SIS junctions attached to a linear network.

network in the frequency domain, constructing the Thevenin or Norton equivalent at each of the harmonic frequencies present in the network. Concurrently a time domain calculation of the response at each nonlinear element is conducted starting with some suitable initial driving function (current or voltage). The results of the two analyses are compared following suitable transformation; differences lead to adjustment of the harmonic signals present at the ports of the linear network and the time domain waveforms used for the driving functions of the nonlinear elements. The process is iterated until reaching convergence of the solutions. Hicks and Khan [5] provide a detailed analysis of this technique and its convergence properties.

In the case of mixers utilizing SIS devices as the nonlinear elements, the traditional harmonic balance approach outlined above has a very serious limitation: the time domain analysis must proceed for many cycles in order to determine the steady-state waveforms, greatly increasing the computation time for each iteration of the procedure. This limitation was overcome by Withington and Kollberg [1] who developed an algorithm for performing the nonlinear analysis of such devices purely in the frequency domain, a technique they refer to as spectral domain analysis. Starting from the mixer theory of Tucker [6], they develop the equations needed to fully analyze the frequency domain current response of a single SIS junction to the set of large-amplitude voltages induced by a dc bias and local oscillator source.

This paper extends the results of Withington and Kollberg to networks containing multiple SIS devices. The large signal solution is found using a multidimensional Newton-Raphson technique to achieve very rapid convergence, even when several harmonics and junctions are included in the analysis. The technique requires the Jacobian matrix of the nonlinear SIS response to changes in the large signal voltages. As will be shown, this matrix can be easily generated from the small signal RF conversion matrix. A final improvement is to conduct the linear circuit calculations using the scattering matrix representation rather than an impedance or admittance representation (which might not exist for certain circuit configurations).

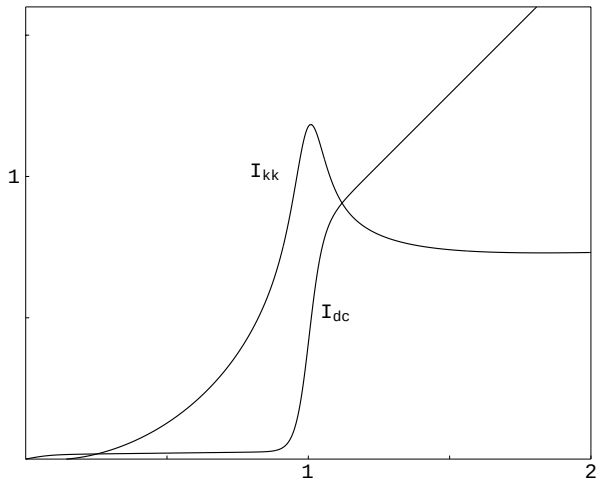

Fig. 2. Typical normalized SIS I-V characteristic curves.

II. The Harmonic Balance Equations

A. Nonlinear Calculation of the Harmonic Currents

To perform the spectral domain analysis of the SIS operating state, the voltages and currents across each junction are represented as:

$$v(t) = V_0 + \mathrm{Re}\left[\sum_{m=1}^{\infty} V_m\, e^{jm\omega_0 t}\right] \quad ; \quad i(t) = I_0 + \mathrm{Re}\left[\sum_{m=1}^{\infty} I_m\, e^{jm\omega_0 t}\right] \tag{1}$$

where V_0 and I_0 are the constant (dc) components, ω_0 is the local oscillator frequency, and the V_m and I_m are complex phasors. In the case where the circuit contains a single junction, the Fourier coefficients in (1) can be represented by the single, complex valued vectors $\mathbf{v}$ and $\mathbf{i}$; if there are multiple junctions, these vectors will still be used, but the individual components will be denoted by V_m^n and I_m^n, where m is the harmonic number ($m = 0$ for the dc component) and n is the junction index, ranging from 1 to the total number of junctions in the circuit. Withington and Kollberg's adaption of Tucker's mixing theory provides an "admittance" representation of an SIS device: the junction currents $\mathbf{i}$ are calculated from the junction voltages $\mathbf{v}$, $\mathbf{i} = \mathbf{i}(\mathbf{v})$.

The currents through an SIS junction may be calculated as follows (*cf.* [1]):

$$I_0 = \mathrm{Re}\left[I_{(0)}\right] \quad ; \quad I_m = I_{(m)} + I^*_{(-m)} \quad , \quad m > 0 \tag{2}$$

where:

$$I_{(m)} = -j \sum_{k=-\infty}^{\infty} C_k C^*_{k+m}\, \mathrm{I}(V_0 + kV_{ph}) \quad , \quad -\infty < m < \infty \tag{3}$$

In this equation V_0 is the junction dc bias voltage, $V_{ph} = (\hbar/e)\,\omega_0$ is the photon voltage of the local oscillator frequency, the C_k are complex phase factors defined below, and $\mathrm{I}(v)$ is the complex dc I-V characteristic function of the junction, $\mathrm{I}(v) \equiv$

$\mathrm{I}_{kk}(v) + j\,\mathrm{I}_{dc}(v)$. $\mathrm{I}_{dc}(v)$ is the measured dc I-V characteristic curve of the junction; $\mathrm{I}_{kk}(v)$ is its Kramers-Kronig transform. A typical $\mathrm{I}_{dc}(v)$, $\mathrm{I}_{kk}(v)$ pair is shown in figure 2, where the curves have been normalized so that the junction's gap voltage and normal resistance are both unity. Various versions of the Kramers-Kronig transform are seen in the literature; the version shown in figure 2 is that due to Tucker, which vanishes at $v = 0$:

$$\mathrm{I}_{kk}(v) = \frac{1}{\pi}\, P \int_{-\infty}^{\infty} \mathrm{I}_{dc}(v') \left(\frac{1}{v' - v} - \frac{1}{v'} \right) dv' \tag{4}$$

where the P denotes the Cauchy principle value of the integral. $\mathrm{I}_{dc}(v)$ is an odd function and $\mathrm{I}_{kk}(v)$ an even function of the voltage v, so that $\mathrm{I}(-v) = \mathrm{I}^*(v)$. The parentheses around the subscripts in (2) and (3) are used to distinguish harmonic indices of Fourier coefficients which range over negative as well as positive values; harmonic indices without the parentheses may take on nonnegative values only. This notation will be used extensively in Section III.

The complex phase factors C_k are defined by:

$$C_k = \lim_{n\to\infty} C_k^n \;\; ; \;\; C_k^0 = \delta_{0,k} \;\; ; \;\; C_k^{n>0} = \sum_{m=-\infty}^{\infty} C_{k-nm}^{n-1} A_{m,n} \tag{5}$$

where $\delta_{0,k}$ is Kronecker's delta and the complex coefficients $A_{m,n}$ are given by:

$$A_{m,n} = J_m(\alpha_n)\, e^{-jm\phi_n} \tag{6}$$

The coefficients α_n and ϕ_n are derived from the magnitude and phase of the harmonic voltage phasor V_n, where the magnitude is normalized by the photon voltage of harmonic n, which is nV_{ph}:

$$\alpha_n\, e^{j\phi_n} \;=\; V_n/(n\, V_{ph}) \tag{7}$$

Expressions (2) to (7) define the harmonic currents I_m through a junction in terms of the harmonic voltages V_n, thereby defining the vector function $\mathbf{i}(\mathbf{v})$. Note that the functions $A_{m,n}$ of the V_n (expressions (6) and (7)) are not analytic; this will be an important consideration when constructing the Jacobian matrix used by the Newton-Raphson algorithm.

B. The Junction Operating States and the Linear Network

The linear embedding network (figure 1) connecting the junctions will be represented as having a port for every junction at every harmonic frequency and dc; its behavior may be represented by a scattering matrix $\mathcal{S}$ and wave source vector $\mathbf{b_s}$. Referring to figure 3, the linear network experiences incoming waves $\mathbf{a}$ and responds by emitting waves $\mathbf{b}$. Because there are active sources embedded in the network (the dc bias and local oscillator), the network will emit waves $\mathbf{b_s}$ in the absence of any

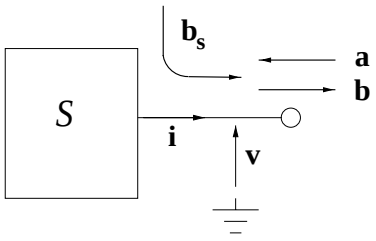

Fig. 3. The scattering matrix representation of a linear network.

incoming waves (as well as noise, which we ignore for the purposes of harmonic balance). Also indicated in figure 3 are the conventional voltages $\mathbf{v}$ and currents $\mathbf{i}$ at the ports. The various vectors are related as follows:

$$\mathbf{b} = \mathbf{b_s} + \mathcal{S}\,\mathbf{a}\;; \quad \mathbf{v} = (\mathbf{b}+\mathbf{a})\sqrt{Z_0}\;; \quad \mathbf{i} = (\mathbf{b}-\mathbf{a})/\sqrt{Z_0} \tag{8}$$

where Z_0 is the normalizing impedance of the scattering representation of the network (usually $50\,\Omega$). A major advantage of the scattering representation over the impedance and admittance representations of a linear network is that it always exists; some common networks have either no impedance representation or no admittance representation. Note that the voltages and currents in (8) are RMS, whereas the vectors of Fourier coefficients from (1) are peak amplitudes. This means that we must be careful about factors of $\sqrt{2}$ for the ac coefficients when solving the harmonic balance equations.

The relationships in (8) where $\mathbf{v}$ and $\mathbf{i}$ are the RMS harmonic voltages and currents through the SIS devices attached to the network lead to the nonlinear system of equations which must be solved by the harmonic balance routine:

$$Z_0(\mathcal{I}+\mathcal{S})\,\mathbf{i}(\mathbf{v}) \;+\; (\mathcal{I}-\mathcal{S})\,\mathbf{v} - 2\sqrt{Z_0}\,\mathbf{b_s} = 0 \tag{9}$$

where $\mathcal{I}$ is the identity matrix. One advantage of this scattering matrix formulation is that the impedance and admittance matrices are not needed; as already mentioned, one or the other of these matrices may not exist. For example, a mixer circuit containing a series array of junctions would not have an impedance representation.

C. Newton-Raphson Iteration Calculations

The Newton-Raphson method for solving a nonlinear system $\mathbf{y}(\mathbf{x}) = 0$ is to replace the estimated solution $\mathbf{x}_i$ with the improved estimate $\mathbf{x}_{i+1} = \mathbf{x}_i + \delta\mathbf{x}_i$, where $\delta\mathbf{x}_i$ is the solution to the *linear* system $(d\mathbf{y}/d\mathbf{x})_{\mathbf{x}_i}\delta\mathbf{x}_i = -\mathbf{y}(\mathbf{x}_i)$, and $(d\mathbf{y}/d\mathbf{x})_{\mathbf{x}_i}$ is the Jacobian matrix of $\mathbf{y}(\mathbf{x})$ evaluated at $\mathbf{x}_i$. This method is quadratically convergent so long as the Jacobian does not vanish at the root and the initial estimate is sufficiently close to the root.

In expression (9), $\mathcal{S}$, $\mathcal{I}$, $\mathbf{b_s}$, and Z_0 are not functions of $\mathbf{v}$ and $\mathbf{i}$, so differentiating with respect to the components of $\mathbf{v}$ results in the following equation for the correction

$\delta\mathbf{v}$ to an estimated $\mathbf{v}$:

$$\left(Z_0(\mathcal{I}+\mathcal{S})\,\frac{d\mathbf{i}}{d\mathbf{v}} \,+\, (\mathcal{I}-\mathcal{S}) \right)\,\delta\mathbf{v} \,=\, 2\sqrt{Z_0}\,\mathbf{b_s} \,-\, Z_0(\mathcal{I}+\mathcal{S})\,\mathbf{i}(\mathbf{v}) \,-\, (\mathcal{I}-\mathcal{S})\,\mathbf{v} \qquad (10)$$

When using (9) and (10) the elements of the source vector $\mathbf{b_s}$ representing ac signals must be multiplied by $\sqrt{2}$ to convert them to peak amplitudes from their RMS values, since these are the relevant quantities in the Tucker theory. The final values of the harmonic currents $\mathbf{i}$ and voltages $\mathbf{v}$ should be divided by $\sqrt{2}$ if their RMS values are required. One must be careful not to apply these corrections to the dc bias values.

The harmonic balance routine will seek a solution to the nonlinear system (9) by first calculating the linear network characteristics $\mathcal{S}$ and $\mathbf{b_s}$. After assuming an initial trial voltage vector $\mathbf{v}$, the routine must update $\mathbf{v}$ by finding the Jacobian matrix $d\mathbf{i}/d\mathbf{v}$ and then solving (10) for the corrections $\delta\mathbf{v}$. The process is repeated until the corrections become sufficiently small. The actual implementation of a satisfactory Newton-Raphson algorithm is somewhat more complicated; it must continually monitor the convergence behavior of the iterations and be prepared to adjust $\delta\mathbf{v}$. Potential difficulties include the algorithm's behavior near saddle points or local extrema of the right hand side of (10).

III. Generating the Jacobian Matrix

A. Basic Properties

In order to use (10) we must form the Jacobian matrix $d\mathbf{i}/d\mathbf{v}$ with elements $\partial I_m^n/\partial V_{m'}^{n'}$ ranging over all pairs of harmonics m and m' and SIS devices n and n'. Since the currents through one device n do not directly depend on the voltages across a different device n', where $n \neq n'$, we know immediately that:

$$\partial I_m^n/\partial V_{m'}^{n'} = \delta_{n,n'}\;\partial I_m^n/\partial V_{m'}^{n} \qquad (11)$$

Unfortunately, because the $A_{m,n}$ defined in (6) are not analytic, it is impossible to define a single complex derivative $\partial I_m/\partial V_{m'}$. The solution chosen here is to define the Jacobian matrix in terms of separate derivatives of the real part and imaginary part of each harmonic current I_m with respect to the real part and imaginary part of each harmonic voltage $V_{m'}$ (recall that harmonic number 0 denotes the dc bias component). These four derivatives are real, not complex, and will be symbolized by:

$$\frac{\partial I_{m\,;\,r}}{\partial V_{m'\,;\,r}} \;\;;\;\; \frac{\partial I_{m\,;\,i}}{\partial V_{m'\,;\,r}} \;\;;\;\; \frac{\partial I_{m\,;\,r}}{\partial V_{m'\,;\,i}} \;\;;\;\; \frac{\partial I_{m\,;\,i}}{\partial V_{m'\,;\,i}} \qquad (12)$$

where the "; r" and "; i" suffixes denote the real and imaginary parts, respectively, of the harmonic voltages or currents.

As for harmonic 0 (the dc bias) the imaginary parts I_0 and V_0 will be assumed to be identically zero. In order to keep the resulting Jacobian from becoming singular,

we set the derivatives as follows:

$$\frac{\partial I_{0\,;\,i}}{\partial V_{m\,;\,r}} = \frac{\partial I_{0\,;\,i}}{\partial V_{m\,;\,i}} = \frac{\partial I_{m\,;\,r}}{\partial V_{0\,;\,i}} = \frac{\partial I_{m\,;\,i}}{\partial V_{0\,;\,i}} = 0 \quad , \quad m > 0 \quad ;$$
$$\frac{\partial I_{0\,;\,i}}{\partial V_{0\,;\,r}} = \frac{\partial I_{0\,;\,r}}{\partial V_{0\,;\,i}} = 0 \quad ; \quad \frac{\partial I_{0\,;\,i}}{\partial V_{0\,;\,i}} = 1 \tag{13}$$

In the actual implementation we apply (13) not to $d\mathbf{i}/d\mathbf{v}$ in (10), but to the entire matrix multiplying $\delta\mathbf{v}$, saving a little time. Another alternative to (13), of course, would simply be to eliminate the imaginary part of the dc bias current and voltage from the equations.

B. Relation to the Small Signal Admittance Matrix

When the SIS junction is used as a heterodyne mixer, the infinitesimal signal voltage and current response can be expressed using the following Fourier expansions:

$$\delta v(t) = \mathrm{Re} \sum_{m=-\infty}^{\infty} \delta V_{(m)}\, e^{j\omega_{(m)}t} \quad ; \quad \delta i(t) = \mathrm{Re} \sum_{m=-\infty}^{\infty} \delta I_{(m)}\, e^{j\omega_{(m)}t} \tag{14}$$

where $\omega_{(m)} = m\omega_0 + \omega_{if}$, and ω_{if} is the IF output frequency. Note that parentheses are used with the harmonic index m since it takes on negative values as well as nonnegative in these expressions. The infinitesimal sideband currents and voltages are linearly related through the small signal RF conversion admittance matrix, $\mathcal{Y}_{(m,m')}$:

$$\delta I_{(m)} = \sum_{m'=-\infty}^{\infty} \mathcal{Y}_{(m,m')} \delta V_{(m')} \tag{15}$$

Clearly this is the case if and only if

$$\mathcal{Y}_{(m,m')} = \frac{\partial I_{(m)}}{\partial V_{(m')}} \tag{16}$$

In the limit of zero IF frequency, $\omega_{(m)} = m\omega_0$, and (14) becomes an alternate form of the harmonic expansions in (1). The relation expressed in (16) provides the connection between $\mathcal{Y}_{(m,m')}$ and the derivatives in (12).

Equating the expansions (1) and (14) we find the relations between the coefficients in the alternate expansions for $i(t)$:

$$I_0 = I_{(0)} \quad ; \quad I_m = I_{(m)} + I^*_{(-m)} \,, \quad m > 0 \tag{17}$$

with a similar relation for the harmonic voltages. Note that $I_{(0)}$ has been arbitrarily chosen to be real with no loss of generality in (14), since $\omega_{if} = 0$.

Consider the real and imaginary parts of I_m, for $m > 0$, using (17):

$$\begin{aligned} I_m &= I_{m\,;\,r} + jI_{m\,;\,i} \,, \quad m > 0 \\ I_{m\,;\,r} &= \left(I_{(m)} + I_{(-m)} + I^*_{(m)} + I^*_{(-m)}\right)/2 \\ I_{m\,;\,i} &= \left(I_{(m)} - I_{(-m)} - I^*_{(m)} + I^*_{(-m)}\right)/2j \end{aligned} \tag{18}$$

Using these expressions and the similar ones for the V_m, we can differentiate (1):

$$\begin{aligned}
dI_m &= dI_{m\,;r} + j\, dI_{m\,;i}\ , \quad m > 0 \\
&= \sum_{m'=0}^{\infty} \left[\left(\frac{\partial I_{m\,;r}}{\partial V_{m'\,;r}} + j \frac{\partial I_{m\,;i}}{\partial V_{m'\,;r}} \right) dV_{m'\,;r} + \left(\frac{\partial I_{m\,;r}}{\partial V_{m'\,;i}} + j \frac{\partial I_{m\,;i}}{\partial V_{m'\,;i}} \right) dV_{m'\,;i} \right] \\
&= \left(\frac{\partial I_{m\,;r}}{\partial V_{0\,;r}} + j \frac{\partial I_{m\,;i}}{\partial V_{0\,;r}} \right) dV_{(0)} \\
&\quad + \frac{1}{2} \sum_{m'=1}^{\infty} \left[\left(\frac{\partial I_{m\,;r}}{\partial V_{m'\,;r}} + j \frac{\partial I_{m\,;i}}{\partial V_{m'\,;r}} - j \frac{\partial I_{m\,;r}}{\partial V_{m'\,;i}} + \frac{\partial I_{m\,;i}}{\partial V_{m'\,;i}} \right) dV_{(m')} \right. \\
&\quad + \left(\frac{\partial I_{m\,;r}}{\partial V_{m'\,;r}} + j \frac{\partial I_{m\,;i}}{\partial V_{m'\,;r}} + j \frac{\partial I_{m\,;r}}{\partial V_{m'\,;i}} - \frac{\partial I_{m\,;i}}{\partial V_{m'\,;i}} \right) dV^*_{(m')} \\
&\quad + \left(\frac{\partial I_{m\,;r}}{\partial V_{m'\,;r}} + j \frac{\partial I_{m\,;i}}{\partial V_{m'\,;r}} + j \frac{\partial I_{m\,;r}}{\partial V_{m'\,;i}} - \frac{\partial I_{m\,;i}}{\partial V_{m'\,;i}} \right) dV_{(-m')} \\
&\quad \left. + \left(\frac{\partial I_{m\,;r}}{\partial V_{m'\,;r}} + j \frac{\partial I_{m\,;i}}{\partial V_{m'\,;r}} - j \frac{\partial I_{m\,;r}}{\partial V_{m'\,;i}} + \frac{\partial I_{m\,;i}}{\partial V_{m'\,;i}} \right) dV^*_{(-m')} \right] \qquad (19)
\end{aligned}$$

where we've made use of the fact that $V_0 = V_{(0)}$ is real.

Performing a similar expansion starting from (17) and using (15) and (16),

$$\begin{aligned}
dI_m &= dI_{(m)} + dI^*_{(-m)}\ , \quad m > 0 \\
&= \sum_{m'=-\infty}^{\infty} \left(\mathcal{Y}_{(m,m')}\, dV_{(m')} + \mathcal{Y}^*_{(-m,m')}\, dV^*_{(m')} \right) \\
&= \left(\mathcal{Y}_{(m,0)} + \mathcal{Y}^*_{(-m,0)} \right) dV_{(0)} \\
&\quad + \sum_{m'=1}^{\infty} \left(\mathcal{Y}_{(m,m')}\, dV_{(m')} + \mathcal{Y}^*_{(-m,m')}\, dV^*_{(m')} \right. \\
&\quad \left. + \mathcal{Y}_{(m,-m')}\, dV_{(-m')} + \mathcal{Y}^*_{(-m,-m')}\, dV^*_{(-m')} \right) \qquad (20)
\end{aligned}$$

Finally consider $I_0 = I_{(0)}$ (real), making use of (13):

$$\begin{aligned}
dI_0 &= dI_{0\,;r} \\
&= \frac{\partial I_{0\,;r}}{\partial V_{0\,;r}}\, dV_0 \ + \ \sum_{m'=1}^{\infty} \left(\frac{\partial I_{0\,;r}}{\partial V_{m'\,;r}}\, dV_{m'\,;r} + \frac{\partial I_{0\,;r}}{\partial V_{m'\,;i}}\, dV_{m'\,;i} \right) \\
&= \frac{\partial I_{0\,;r}}{\partial V_{0\,;r}}\, dV_{(0)} \\
&\quad + \frac{1}{2} \sum_{m'=1}^{\infty} \left[\left(\frac{\partial I_{0\,;r}}{\partial V_{m'\,;r}} - j \frac{\partial I_{0\,;r}}{\partial V_{m'\,;i}} \right) dV_{(m')} + \left(\frac{\partial I_{0\,;r}}{\partial V_{m'\,;r}} + j \frac{\partial I_{0\,;r}}{\partial V_{m'\,;i}} \right) dV^*_{(m')} \right. \\
&\quad \left. + \left(\frac{\partial I_{0\,;r}}{\partial V_{m'\,;r}} + j \frac{\partial I_{0\,;r}}{\partial V_{m'\,;i}} \right) dV_{(-m')} + \left(\frac{\partial I_{0\,;r}}{\partial V_{m'\,;r}} - j \frac{\partial I_{0\,;r}}{\partial V_{m'\,;i}} \right) dV^*_{(-m')} \right] \qquad (21)
\end{aligned}$$

and

$$\begin{aligned} dI_0 &= dI_{(0)} = dI^*_{(0)} = \left(dI_{(0)} + dI^*_{(0)}\right)/2 \\ &= \mathcal{Y}_{(0,0)} dV_{(0)} \\ &+ \frac{1}{2}\sum_{m'=1}^{\infty} \left(\mathcal{Y}_{(0,m')}\, dV_{(m')} + \mathcal{Y}^*_{(0,m')}\, dV^*_{(m')} \right. \\ &\left. + \mathcal{Y}_{(0,-m')}\, dV_{(-m')} + \mathcal{Y}^*_{(0,-m')}\, dV^*_{(-m')}\right) \end{aligned} \tag{22}$$

Comparing (19) to (22) we find the following relations between the derivatives (12) needed for the Jacobian matrix and the small signal admittance matrix $\mathcal{Y}_{(m,m')}$ (when $\omega_{if} = 0$):

$$\mathcal{Y}_{(-m,-m')} = \mathcal{Y}^*_{(m,m')} \tag{23}$$

$$\frac{\partial I_{0\,;r}}{\partial V_{0\,;r}} = \mathcal{Y}_{(0,0)} \tag{24}$$

$$\frac{\partial I_{0\,;r}}{\partial V_{m'\,;r}} = \mathrm{Re}\,\mathcal{Y}_{(0,m')} \qquad \frac{\partial I_{0\,;r}}{\partial V_{m'\,;i}} = -\mathrm{Im}\,\mathcal{Y}_{(0,m')} \tag{25}$$

$$\frac{\partial I_{m\,;r}}{\partial V_{0\,;r}} = 2\,\mathrm{Re}\,\mathcal{Y}_{(m,0)} \qquad \frac{\partial I_{m\,;i}}{\partial V_{0\,;r}} = 2\,\mathrm{Im}\,\mathcal{Y}_{(m,0)} \tag{26}$$

$$\frac{\partial I_{m\,;r}}{\partial V_{m'\,;r}} = \mathrm{Re}\left(\mathcal{Y}_{(m,m')} + \mathcal{Y}_{(m,-m')}\right) \qquad \frac{\partial I_{m\,;i}}{\partial V_{m'\,;r}} = \mathrm{Im}\left(\mathcal{Y}_{(m,m')} + \mathcal{Y}_{(m,-m')}\right) \tag{27}$$

$$\frac{\partial I_{m\,;r}}{\partial V_{m'\,;i}} = -\mathrm{Im}\left(\mathcal{Y}_{(m,m')} - \mathcal{Y}_{(m,-m')}\right) \qquad \frac{\partial I_{m\,;i}}{\partial V_{m'\,;i}} = \mathrm{Re}\left(\mathcal{Y}_{(m,m')} - \mathcal{Y}_{(m,-m')}\right) \tag{28}$$

where $m > 0$ and $m' > 0$ in (25) to (28).

C. Calculating the Small Signal Admittance Matrix

The small signal admittance matrix $\mathcal{Y}_{(m,m')}$ must be calculated in order to perform the RF conversion analysis of a heterodyne receiver. Tucker's theory provides the following expressions for $\mathcal{Y}_{(m,m')}$ in the case of an SIS mixer:

$$\begin{aligned} &\mathcal{Y}_{(m,m')} = \\ &\quad \frac{-j}{2(m'V_{ph} + V_{if})} \sum_{k=-\infty}^{\infty} C_k C^*_{k+m-m'} \left[\mathrm{I}(V_0 + kV_{ph}) - \mathrm{I}(V_0 + (k-m')V_{ph} - V_{if}) \right. \\ &\qquad \left. - \mathrm{I}^*(V_0 + (k+m)V_{ph} + V_{if}) + \mathrm{I}^*(V_0 + (k+m-m')V_{ph})\right] \end{aligned} \tag{29}$$

where $V_{if} = (\hbar/e)\omega_{if}$ is the photon voltage of the IF frequency ω_{if}.

For $\omega_{if} = 0$, expression (29) becomes:

$$\mathcal{Y}_{(m,m'\neq 0)} = \frac{-j}{2m'V_{ph}} \sum_{k=-\infty}^{\infty} C_k C^*_{k+m-m'} \left[\mathrm{I}(V_0 + kV_{ph}) - \mathrm{I}(V_0 + (k-m')V_{ph}) - \mathrm{I}^*(V_0 + (k+m)V_{ph}) + \mathrm{I}^*(V_0 + (k+m-m')V_{ph}) \right] \tag{30}$$

$$\mathcal{Y}_{(m,0)} = \frac{-j}{2} \sum_{k=-\infty}^{\infty} C_k C^*_{k+m-m'} \left[\mathrm{I}'(V_0 + kV_{ph}) - \mathrm{I}'^*(V_0 + (k+m)V_{ph}) \right] \tag{31}$$

The primes ($'$) on the currents in (31) denote derivatives of the I-V characteristic curves (figure 2) with respect to voltage. A little effort with index manipulation in (30) and (31) would suffice to show that these expressions satisfy (23). Now we have all the information needed to perform the Newton-Raphson iteration (10).

D. Final Considerations

Once routines to calculate $\mathbf{i}(\mathbf{v})$ and the $\mathcal{Y}_{(m,m')}$ have been developed, along with more traditional circuit routines to determine the linear embedding network behaviors $\mathcal{S}$ and $\mathbf{b_s}$, the harmonic balance routine may be implemented. Expressions (9) and (10) define the complex vector function of $\mathbf{v}$ and its Jacobian which are used by the Newton-Raphson solver to perform the harmonic balance. The vectors and matrices involved are potentially large, having dimension $N = n_j(m_{max}+1)$, where n_j is the number of SIS junctions in the circuit and m_{max} is the number of harmonics to be included in the analysis; each element must hold a pair of real numbers to represent the complex quantities involved.

The potentially most time-consuming calculation in these expressions is the matrix multiplication $(\mathcal{I}+\mathcal{S})(d\mathbf{i}/d\mathbf{v})$ in the formula for the Jacobian. This calculation is not as bad as it seems, however, because the matrices involved are block-diagonal. This characteristic was previously described for $d\mathbf{i}/d\mathbf{v}$ in expression (11). Consider the elements of the matrices $(\mathcal{I} \pm \mathcal{S})$. Since the embedding network is linear, it cannot connect signals with different frequencies; therefore the elements of $\mathcal{S}$ must look like (using the same index notation as in (11)):

$$S^{n,n'}_{m,m'} = \delta_{m,m'}\, S^{n,n'}_{m} \tag{32}$$

The elements of the matrix product in (10) are therefore:

$$\begin{aligned} \left[(\mathcal{I}+\mathcal{S}) \frac{d\mathbf{i}}{d\mathbf{v}} \right]^{n,n'}_{m,m'} &= \sum_{n'',m''} \left(\delta_{n,n''}\delta_{m,m''} + \delta_{m,m''}\, S^{n,n''}_{m} \right) \delta_{n'',n'} \frac{\partial I^{n'}_{m''}}{\partial V^{n'}_{m'}} \\ &= (\delta_{n,n'} + S^{n,n'}_{m}) \frac{\partial I^{n'}_{m}}{\partial V^{n'}_{m'}} \end{aligned} \tag{33}$$

and no summing over an index is required to perform the multiplication.

IV. Implementation and Results

Routines to perform the calculations outlined above have been implemented and included in an extensive C++ class library (named "SuperMix") used to model SIS mixers and receivers. This library includes a complete complex linear algebra capability as well as a multiparameter optimizer and is described in more detail in [7]. It can perform gain and noise analyses of superconducting and conventional circuitry of arbitrary complexity, including superconducting surface impedance calculations and modeling of HEMT amplifiers. The source code of this library will be made freely available. It compiles under the Free Software Foundation's freely available compiler *g++* and has been tested on Linux (Pentium) and Sun UltraSparc platforms.

Twin-slot, two-junction mixers as described in [8] have been modeled using SuperMix. A schematic block diagram of the circuit model is illustrated in figure 4. Not shown is the dc bias circuit for the two junctions, which is modeled as an ideal voltage source (battery). Note that the entire RF superconducting circuitry is included in the model, including both SIS junctions. To illustrate some of the capabilities of the library interface, we have included figure 5, which shows the short C++ file which fully specifies the physical design parameters of the twin-slot circuitry to SuperMix. The `parameter` objects declared in the file are given initial values which may be modified by the program. Because the circuit parameters are modifiable, SuperMix's optimizer may be used to adjust them during program execution. The illustrated specification file is for a "device 63", which is a mixer designed for operation in the 600 to 700 GHz range and which is described in detail in [8]. The SIS I-V characteristics used are those shown in figure 2; SuperMix scales these normalized curves using the SIS parameter data provided in the specification file.

Figure 6 shows various dc current-voltage characteristic curves predicted by the model. The pumped curves show the effect of varying local oscillator (LO) frequency around the design frequency of 650 GHz; the LO power at the antenna was held constant at 200 nW. In this and subsequent figures the currents shown are the total bias currents obtained by summing the currents from each of the two SIS junctions. The values of these currents are found in elements of $\mathbf{i}(\mathbf{v})$ following a successful harmonic balance calculation. Even though each harmonic balance considered both junctions and three harmonic frequencies, the Newton-Raphson technique required an average of only four iterations to converge to about 0.1% or better accuracy. On average, a full harmonic balance took approximately 0.015 seconds to complete using a 333 Mhz Sun Ultra 10 workstation (6.3 seconds total execution time; 324 harmonic balances were required).

Figure 7 shows hot and cold load (RF background temperature) total IF output power into 100 MHz bandwidth centered at 6 GHz. The LO power was set to 200 nW at the antenna, with a frequency of 650 GHz. As with the other simulations shown, the LO fundamental frequency plus two harmonics were included in each harmonic balance and subsequent mixer analysis. The noise effects of the associated optics and IF stage were not included in the figure 7 analysis, although SuperMix is fully capable of including their effects as well. The curves were obtained by performing

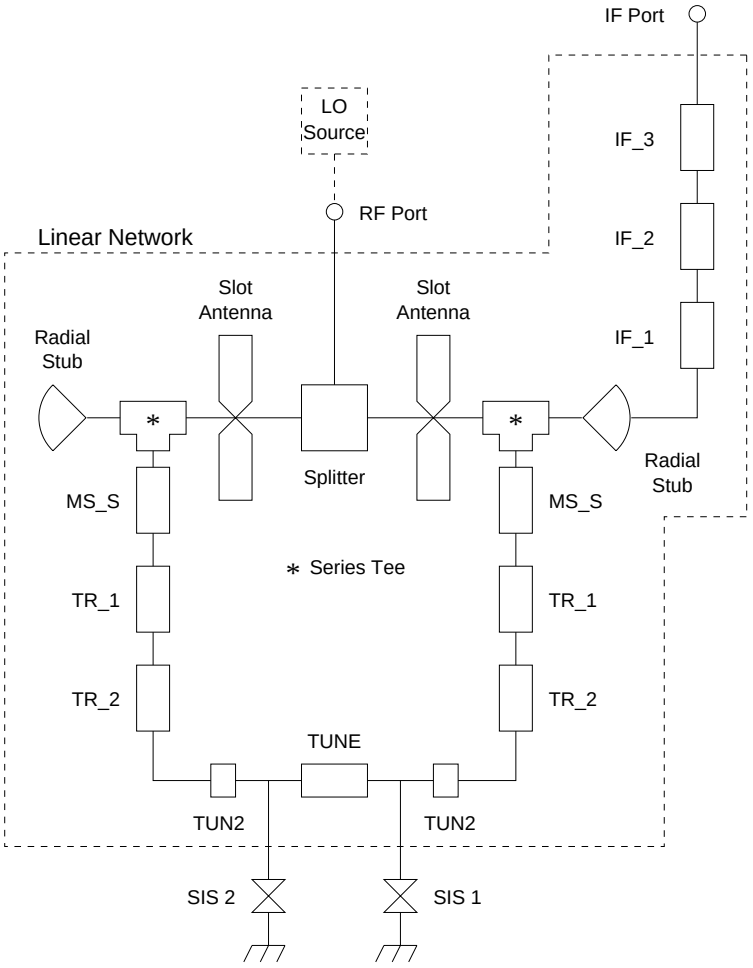

Fig. 4. Schematic block diagram of the twin-slot, two-junction mixer circuit used for the examples. Each labeled block is a circuit element. Several of the labels correspond to the names used in the SuperMix specification file shown in figure 5 and represent superconducting transmission line elements. The splitter is an ideal power splitter which is used to feed the RF and LO signals equally to the two slot antennas.

two complete harmonic balances (for the unpumped and pumped conditions) and two complete RF conversion analyses, including conversion gain and noise calculations, at each of 81 bias points. The total execution time was under 10 seconds, of which approximately 1.5 seconds were required for initialization (reading data files and building interpolation tables), again on a 333 Mhz Sun Ultra 10 workstation.

As a final example, figure 8 compares a calculated Fourier-Transform Spectrometer (FTS) response with a measured response for a device 63 twin-slot mixer. The FTS technique is described in detail in [8]. FTS "response" is defined as the change in mixer bias current in response to a large change in the RF background source temperature as a function of RF frequency, normalized to arbitrary units in which the peak response is set to approximately unity. There is no separate local oscillator source; the background RF thermal energy serves as a very weak local oscillator

```
// 63 Device specification file
// 2/1/99 FRR


// The superconductors used:
const sc_material & GP_MATERIAL  = nb;      // niobium ground plane material
const sc_material & TOP_MATERIAL = nb;      // niobium top strip material

// SIS junction parameters
parameter RNA  = 19.9*Ohm*Micron*Micron;    // normal resistance - area product
parameter SCAP = 85.0*fFarad/Micron/Micron; // specific capacitance (per area)
parameter AREA = 1.3*1.3*Micron*Micron;     // effective junction area
parameter VGAP = 2.8*mVolt;                 // SIS gap voltage
parameter VBIAS = 2.4*mVolt;                // SIS bias voltage
const char * const IDC_FILE = "72_idc.dat"; // DC IV characteristic (normalized to Vgap and Rn)
const char * const IKK_FILE = "72_ikk.dat"; // Kramers-Kronig transform of the DC IV curve

// layer thicknesses:
parameter GP_THICKNESS   = 2000.*Angstrom;  // ground plane
parameter TOP_THICKNESS  = 2000.*Angstrom;  // top strip
parameter MS_THICKNESS   = 4000.*Angstrom;  // SiO layer generally
parameter TUNE_THICKNESS = 2000.*Angstrom;  // SiO in tuning inductor

// Microstrip dimensions (width,length) (each entry is a parameter):
wl TR_1 = { 2.0*Micron, 37.7*Micron };      // transformer section 1
wl TR_2 = { 4.5*Micron, 41.1*Micron };      // transformer section 2
wl MS_S = { 2.0*Micron, 2.5*Micron };       // bit between radial stub and TR_1
wl IF_1 = { 2.0*Micron, 44.0*Micron };      // if section 1 (nearest radial stub)
wl IF_2 = { 10.0*Micron, 41.*Micron };      // if section 2
wl IF_3 = { 10.0*Micron,  1.0*Micron };     // if section 3 (nearest IF output)
wl TUNE = { 5.0*Micron, 9.8*Micron };       // full length of tuning inductor
wl TUN2 = { 5.0*Micron, 2.5*Micron };       // tuning inductor between transformer and SIS

// 90 degree radial stub dimensions:
parameter STUB_R   = 36.0*Micron;           // radial stub radius
parameter STUB_L   = 2.5*Micron;            // length of strip from antenna into stub

// Local Oscillator and IF output parameters:
parameter LO_POWER = 50*Nano*Watt;          // the LO power at the antenna
parameter LO_FREQ  = 650.0*GHz;             // the LO frequency
parameter LO_TEMP  = 0.0*Kelvin;            // thermal noise source temperature at input
parameter IF_FREQ  = 6*GHz;                 // the IF frequency
complex_parameter IF_TERM = complex(50*Ohm);// the input impedance of the IF amplifier

// The antenna impedance information (these cannot change during runtime):
const char * const ANT_FILE = "Zslot.750";  // antenna impedance file name
const double ANT_FILE_FREQ  = 750.0*GHz;    // antenna center frequency used in the file data
const double ANT_TUNE_FREQ  = 650.0*GHz;    // the actual antenna design center frequency

// Mixer calculations:
int HARMONICS = 3;

// The receiver temperature (remains constant during runtime):
const double TEMPERATURE = 4.0*Kelvin;
```

Fig. 5. SuperMix specification file for the twin-slot mixer shown in figure 4. Nearly all of the numerical values may be modified as required during program execution; this file provides initial or default values.

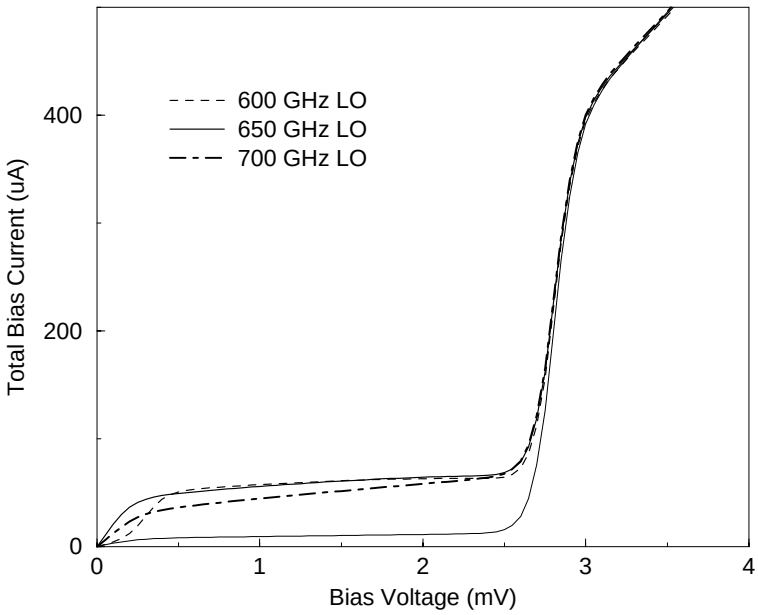

Fig. 6. Calculated pumped IV curves for a 650 GHz twin-slot, two-junction mixer. LO power 200 nW. The unpumped curve is also shown. The sum of the bias currents for the two junctions was calculated every 0.05 mV for a total of 324 points for the four curves. Each point required a full harmonic balance using 3 harmonics. The total execution time was 6.3 seconds on a 333 MHz *Sun Ultra 10*.

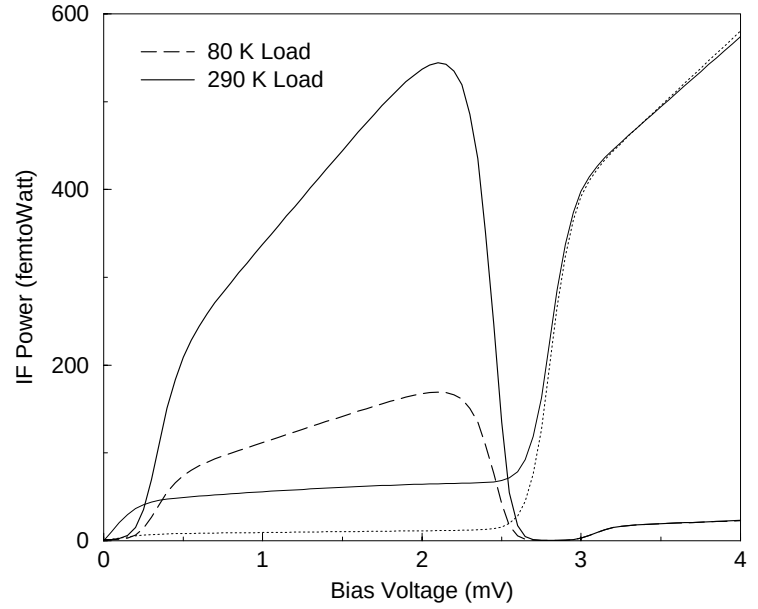

Fig. 7. Calculated hot and cold load IF power curves into a 200 MHz IF bandwidth centered at 6 GHz for a 650 GHz twin-slot mixer. LO power 200 nW. The IV curves are also shown. Only the superconducting mixer circuitry is modeled; noise contributions of the optics and IF amplifier are not included. Required 162 complete harmonic balance calculations and 162 mixer gain and noise analyses; execution time was under 10 seconds on a 333 MHz *Sun Ultra 10*.

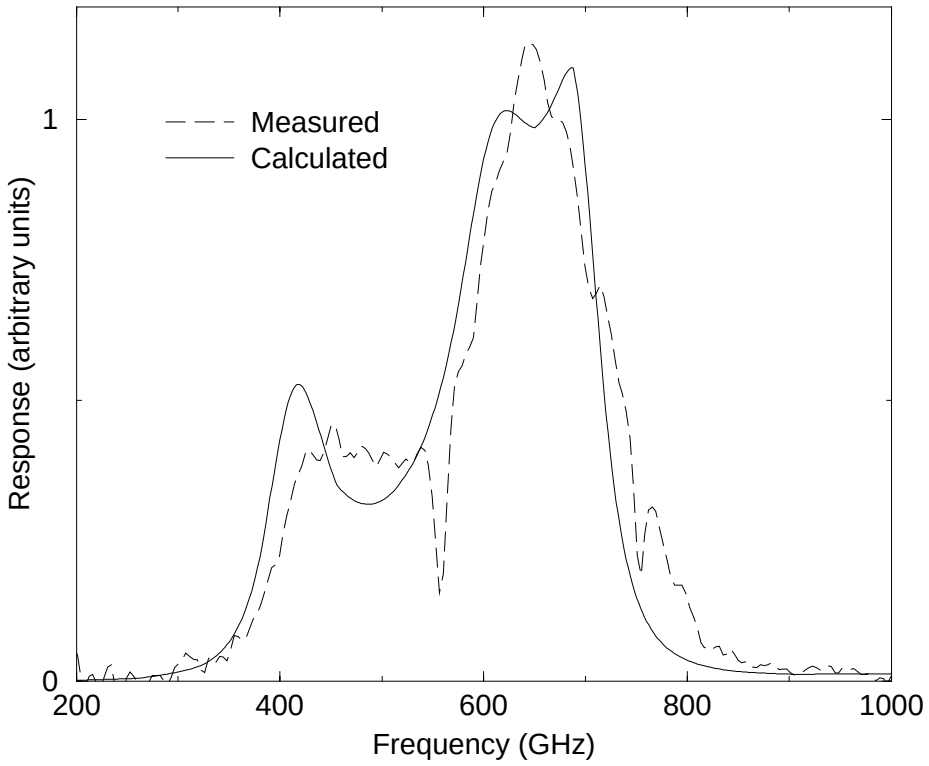

Fig. 8. Calculated and measured FTS response curves for a 650 GHz twin-slot mixer (device 63). Bias voltage was 2.0 mV. 802 harmonic balances were required to calculate the curve shown; execution time was 11.7 seconds. The text describes how the simulated response was calculated; at the peak, the calculated change in bias current is only 3 parts in 10^6.

which slightly pumps the junctions in the mixer. To model this measurement using SuperMix, the program balances the mixer for a very small LO power (0.1 picoWatt was used to generate figure 8); it then rebalances the mixer with the LO source turned off. The resultant change in the total calculated dc bias current drawn by the two junctions is then output as a function of LO frequency. The calculated current differences in the simulation are extremely small—only 31 picoAmps at the peak of the curve (3 parts in 10^6). The fidelity of the result demonstrates the precision of the harmonic balance calculations. The curve shown was calculated every 2 MHz, requiring 802 total harmonic balances. Execution time was 11.7 seconds, again giving 0.015 seconds per harmonic balance. The similarity of the calculated and measured responses is evident in the figure 8; it is important to note that no adjustment of free parameters was done to the mixer model in order to optimize the match of the curves; the parameters shown in figure 5 were the values used by the simulation, except that the bias voltage was set to 2.0 mV to match that used for the measured response. The only adjustment was to uniformly scale the calculated bias current responses (following the program run) to match the scaling used by the measured data.

Acknowledgements

This work was supported in part by NASA/JPL and its Center for Space Microelectronics Technology, by NASA grants NAG5–4890, NAGW–107, and NAG2–1068, by the NASA/USRA SOFIA instrument development program, and by the Caltech Submillimeter Observatory (NSF grant AST–9615025).

References

[1] S. Withington and E. Kollberg, "Spectral-domain analysis of harmonic effects in superconducting quasiparticle mixers," *IEEE Trans. Microwave Theory Tech.*, vol. 37, pp. 231–238, 1989.

[2] A. Kerr, S.-K. Pan, and H. LeDuc, "An integrated sideband separating SIS mixer for 200–280 GHz," *Proc. Ninth International Symposium on Space Terahertz Tech.*, pp. 215–221, 1998.

[3] S.-C. Shi, T. Noguchi, J. Inatani, Y. Irimajiri, and T. Saito, "Experimental results of SIS mixers with distributed junction arrays," *Proc. Ninth International Symposium on Space Terahertz Tech.*, pp. 223–234, 1998.

[4] G. Chattopadhyay, D. Miller, and J. Zmuidzinas, "A 550 GHz dual polarized quasi-optical SIS mixer," *Proc. Tenth International Symposium on Space Terahertz Tech.*, 1999.

[5] R. Hicks and P. Khan, "Numerical analysis of nonlinear solid-state device excitation in microwave circuits," *IEEE Trans. Microwave Theory Tech.*, vol. 30, pp. 251–259, 1982.

[6] J. Tucker, "Quantum limited detection in tunnel junction mixers," *IEEE Jour. Quantum Electronics*, vol. 15, pp. 1234–1258, 1979.

[7] J. Ward, F. Rice, and J. Zmuidzinas, "SuperMix: a flexible software library for high-frequency circuit simulation, including SIS mixers and superconducting components," *Proc. Tenth International Symposium on Space Terahertz Tech.*, 1999.

[8] M. Gaidis, H. LeDuc, M. Bin, D. Miller, J. Stern, and J. Zmuidzinas, "Characterization of low-noise quasi-optical SIS mixers for the submillimeter band," *IEEE Trans. Microwave Theory Tech.*, vol. 44, pp. 1130–1139, 1996.